Probing the remarkable thermal kinetics of visual rhodopsin with E181Q and S186A mutants

Ying Guo,[a] Heidi P. Hendrickson, Pablo E. Videla, Ya-Na Chen, Junming Ho,[b] Sivakumar Sekharan,[c] Victor S. Batista, John C. Tully, and Elsa C. Y. Yan[d]
Department of Chemistry, Yale University, 225 Prospect Street, New Haven, Connecticut 06520, USA

(Received 27 March 2017; accepted 19 May 2017; published online 7 June 2017)

We recently reported a very unusual temperature dependence of the rate of thermal reaction of wild type bovine rhodopsin: the Arrhenius plot exhibits a sharp "elbow" at 47 °C and, in the upper temperature range, an unexpectedly large activation energy (114 ± 8 kcal/mol) and an enormous prefactor ($10^{72\pm5}$ s^{-1}). In this report, we present new measurements and a theoretical model that establish convincingly that this behavior results from a collective, entropy-driven breakup of the rigid hydrogen bonding networks (HBNs) that hinder the reaction at lower temperatures. For E181Q and S186A, two rhodopsin mutants that disrupt the HBNs near the binding pocket of the 11-*cis* retinyl chromophore, we observe significant decreases in the activation energy (~90 kcal/mol) and prefactor (~10^{60} s^{-1}), consistent with the conclusion that the reaction rate is enhanced by breakup of the HBN. The results provide insights into the molecular mechanism of dim-light vision and eye diseases caused by inherited mutations in the rhodopsin gene that perturb the HBNs. *Published by AIP Publishing.* [http://dx.doi.org/10.1063/1.4984818]

INTRODUCTION

Rhodopsin is an effective dim-light photoreceptor, in part, because it is extremely resistant to thermal reaction, i.e., thermal isomerization of the 11-*cis* retinyl chromophore (illustrated in Fig. 1), which can generate the same physiological response as photo-isomerization and thereby lead to false signals (dark noise), is exceedingly slow at physiological temperatures.[1] Since thermal stability is key to rhodopsin's function of dim-light vision, thermal properties of rhodopsin have long been a subject of interest.[2–7] In order to better understand the factors responsible for rhodopsin's thermal stability, we previously carried out measurements of the rate of decay as a function of temperature for wild type (WT) bovine rhodopsin over the temperature range 37.0 – 64.6 °C. As we reported,[8] the resulting Arrhenius plot exhibits a distinct elbow at about 47 °C. In the lower temperature range 37.0–44.5 °C, the Arrhenius parameters were found to be relatively "normal" with activation energy $E_a = 22 \pm 2$ kcal/mol and prefactor $A_{pref} = 10^{9\pm1}$ s^{-1}. Between 52.0 and 64.6 °C, the observed rates again fit quite well to an Arrhenius straight line, but with a markedly different slope, resulting in $E_a = 114 \pm 8$ kcal/mol and $A_{pref} = 10^{72\pm5}$ s^{-1}. These results were unexpected. The barrier along the minimum energy path for a thermal reaction is expected to be equal to or lower than the minimum energy required for photoisomerization, and yet our measured thermal activation energy of 114 kcal/mol is about twice the photon energy required to trigger photoisomerization. Moreover, the prefactor, $10^{72\pm5}$ s^{-1}, is enormous, more than 40 orders of magnitude larger than any previously reported prefactor for a localized unimolecular rate process of which we are aware, and clearly unrelated to the timescale of atomic motion, typically of order 10^{13} s^{-1}. These Arrhenius parameters result from a fit over a relatively small temperature range (~12 °C) and have no meaning when extrapolated beyond this range. Nevertheless, they signal a transition from a localized reaction of the retinyl chromophore at lower temperatures to a more global, collective response involving the surrounding protein and solvent above 52 °C. Structural studies of rhodopsin have revealed water molecules in the transmembrane domain that can form an extended hydrogen bonding network (HBN) with the backbone and polar residues.[9–12] In our prior publication, we hypothesized that the barrier to thermal reaction (the free energy of activation) is increased due to this rigid HBN, thereby impeding isomerization.[8] We concluded that at temperatures between 52.0 and 64.6 °C, approaching the 68.8 °C melting temperature of WT rhodopsin, the free energy of activation is reduced by disordering the protein, i.e., by disrupting the hydrogen bonding networks (HBNs). This is at the expense of an increased enthalpy of breaking hydrogen bonds but is compensated by the large entropy of disorder. The resulting higher enthalpy and entropy of activation are manifested as a high activation energy and prefactor, respectively.

In this paper, we present new experimental results and a theoretical model that confirm this picture and place it on a firm footing. We extend the temperature-dependent rate measurements to two single-site mutants, S186A and E181Q, that

[a] Current address: School of Science and Technology, Georgia Gwinnett College, 1000 University Center Lane, Lawrenceville, GA 30043, USA.
[b] Current address: Institute of High Performance Computing, 1 Fusionopolis Way, #16-16 Connexis North, Singapore 138632.
[c] Current address: Cambridge Crystallographic Data Centre, Center for Integrative Proteomics Research, Rutgers University, 174 Frelinghuysen Road, Piscataway, NJ 08854, USA.
[d] Author to whom correspondence should be addressed: elsa.yan@yale.edu

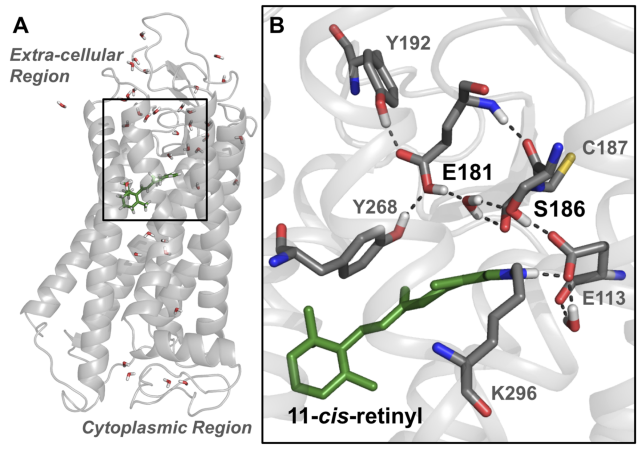

FIG. 1. QM/MM computational structure of rhodopsin. (a) The QM/MM optimized structure of rhodopsin containing 37 water molecules. The 11-*cis*-retinyl chromophore is shown as green sticks. (b) Magnification of the 11-*cis*-retinyl chromophore binding site highlighting residues involved in the protonated Schiff base hydrogen bond network (dashes). The S186 and E181 sites are altered in the mutations.

perturb the hydrogen bonding network in proximity to the retinal chromophore (see Fig. 1). We find that, while still large, the Arrhenius parameters for the two mutants in the higher temperature regime are significantly reduced compared to those for WT. This supports the hypothesis that the large observed Arrhenius parameters result, at least in part, from breaking hydrogen bonds—there are fewer to break in the mutants. In addition, we find that the reaction rate for WT is slowed at all temperatures when the solvent water is replaced by deuterated water, in agreement with the expectation that deuterium strengthens hydrogen bonds.[13]

We present below a theoretical model, supported by quantum mechanics/molecular mechanics (QM/MM) calculations,[14] that reproduces the observed elbows in the Arrhenius plots, the deviations between WT and mutants, and the large activation energies and huge prefactors in the upper temperature range. The model correctly incorporates the dependence of the thermal rate constants on the differences in reaction barrier heights for intact and disordered HBNs and on the enthalpy and entropy of disordering the protein. Furthermore the model, in concert with our experimental results, provides a quantitative estimate of the enhancement in stability of rhodopsin provided by the HBN and therefore the contribution of the HBN to achieving the extremely low dark noise essential for dim-light vision.[15] Mutations in rhodopsin that perturb the HBN can therefore lower the energy barrier for thermal isomerization, introducing dark noise that jeopardizes dim-light vision.[16–18] Over 100 inherited mutations in the rhodopsin gene have been identified to cause retinitis pigmentosa, a group of degenerative diseases.[19] Some of these mutations indeed have been shown to increase the rate of thermal isomerization,[20–22] likely associated with the early symptoms of night blindness. Hence, our theoretical analysis of experimental thermal kinetics of rhodopsin underpins the importance of hydrogen bonding interactions in dim-light vision and provides a quantitative perspective in investigating the molecular mechanism of some inherited eye diseases.

EXPERIMENTAL METHODS

Materials

Mouse monoclonal 1D4 antibody, specific to the C-terminus of rhodopsin, was purchased from the University of British Columbia. 1D5 peptide (TETSQVAPA, corresponding to the last 9 residues of C-terminal) was synthesized by the Keck Biotechnology Resource Laboratory at Yale University. All other chemicals were purchased from Sigma-Aldrich Inc.

Expression and purification of rhodopsin

Our procedures for preparing rhodopsin can be found in detail elsewhere.[17] Stable cell lines of HEK293S expressing WT bovine opsin and the E181Q and S186A mutants were made as described. Rhodopsin samples were purified using the immunoaffinity method. The rhodopsin samples were then concentrated to ~20 μM in 50 mM sodium phosphate (pH 6.5) and 0.1% *n*-dodecyl-β-d-maltoside (DDM) (buffer A) for the experiments.

Sample preparation for D_2O experiments

Rhodopsin at ~0.3 mM in buffer A at a volume of 500 μl was concentrated to 20 μl in a Biomax-30K NMWL centrifugal tube (0.5 ml, Millipore). After concentration, the sample was diluted with buffer C (50 mM sodium phosphate in D_2O, 0.02% DM, pH 6.5) back to ~0.3 mM and stored in buffer C overnight. Buffer C contained lower detergent concentration to account for the increased concentration of detergent after concentration. The following day, the sample was concentrated to ~2.5 mM for the experiments.

Reaction rate measurements

We previously reported that rhodopsin undergoes thermal decay via two pathways: (1) the retinyl chromophore first isomerizes to form a Meta II-like product and then the protonated Schiff base (PSB) of the all-*trans* retinyl chromophore hydrolyzes and (2) the PSB hydrolyzes first resulting in the free 11-*cis* retinal and then 11-*cis* retinal isomerizes in the presence of opsin.[18] In this paper, we report only the total rates of thermal decay, and not the branching ratios of the two individual pathways, which will be examined in a subsequent publication. We measured the rates of thermal decay of E181Q and S186A mutants as well as the decay of WT in D_2O (WT-D_2O) by monitoring the decrease of absorbance at the absorption maximum (508 nm for E181Q and 500 nm for WT, WT-D_2O, and S186A) at different temperatures. To initiate thermal decay, at time $t = 0$ ice-cold concentrated sample was added to a preheated buffer incubated at the desired temperature to a final concentration around 1 μM. A series of UV-visible absorption spectra were taken at various time points. Examples are shown in Figs. 2(a)–2(d). Over time, the optical density at 500 nm for WT rhodopsin and S186A (OD_{500}) or 508 nm for E181Q (OD_{508}) decreases, indicating the decrease in concentration of dark-state samples. Meanwhile, OD_{380} increases due to the formation of free 11-*cis* retinal, all-*trans* retinal bound to opsin, and/or free all-*trans* retinal. The spectra were normalized to OD_{280} to account for solvent evaporation and then to OD_{500} or OD_{508} at $t = 0$. Normalized OD_{500} or OD_{508} was

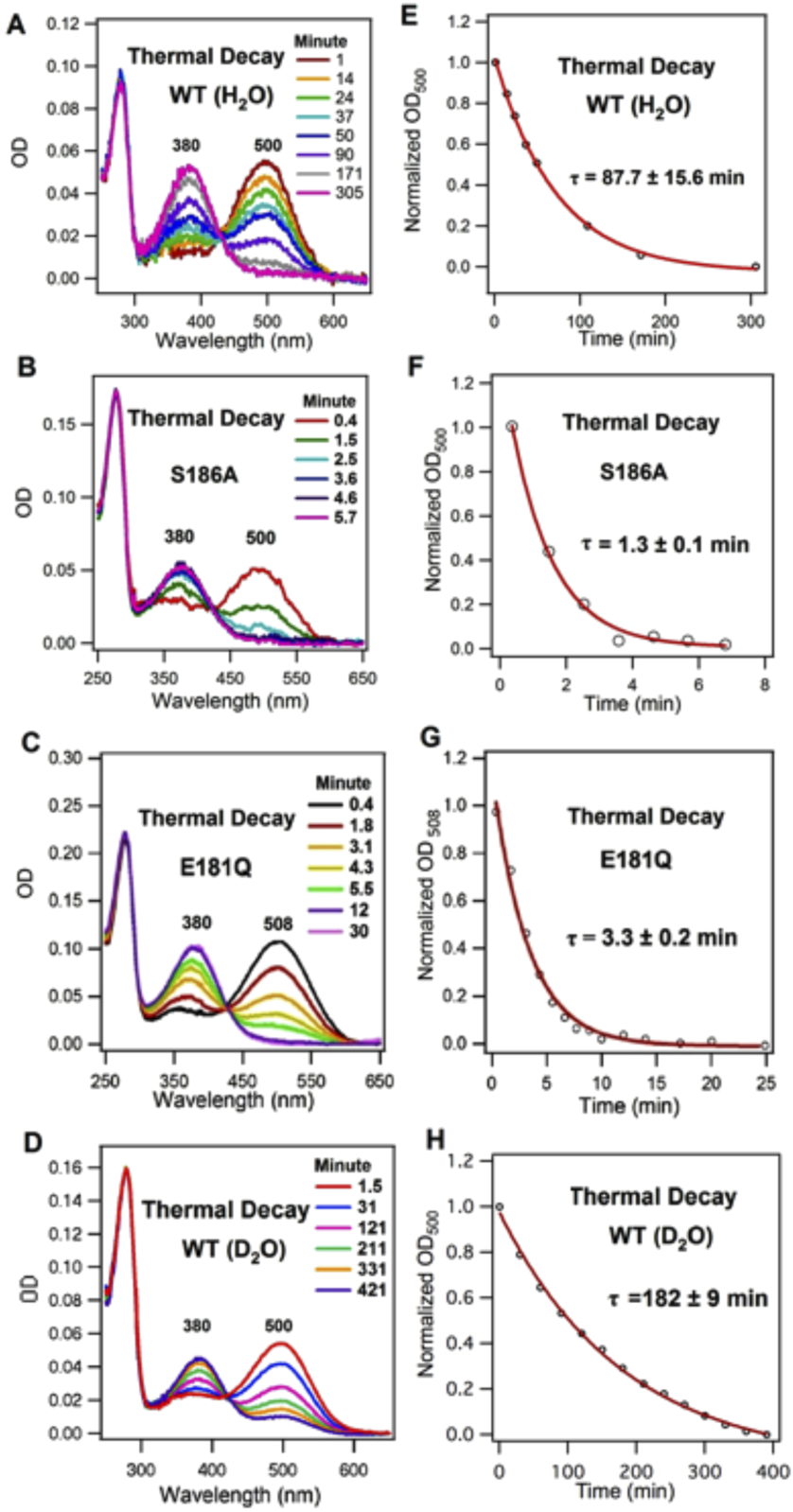

FIG. 2. Thermal reactions of E181Q, S186A, WT in H_2O, and WT in D_2O at 55.0 °C. Time-dependent UV-visible spectra of thermal decay of (a) WT in H_2O, (b) S186A, (c) E181Q, and (d) WT in D_2O. [(e)-(h)] Normalized OD_{508} or OD_{500} plotted as a function of time and fitted to a single exponential function (red).

plotted as a function of time and fitted to a single exponential function to yield the decay times [Figs. 2(e)–2(h)].

Measurements of temperature, enthalpy, and entropy of melting

Because the proposed mechanism for reaction in the higher temperature regime involves partial or complete breakup of the HBN, it is important to measure the enthalpies and entropies associated with this breakup, i.e., the melting parameters. Melting curves of dark-state rhodopsin and its mutants were obtained by circular dichroism spectroscopy described previously.[8] Molar ellipticity at 222 nm ($\theta_{222\,nm}$) was monitored while the temperature of the sample was increased at constant rates of 90 °C/h and 120 °C/h. An increase of

ellipticity reflects disappearance of the α-helix structure, i.e., melting. The melting curves were analyzed using the van't Hoff equation[23] to extract the temperature, T_m, enthalpy, ΔH_m, and entropy, ΔS_m, of melting, as described elsewhere.[8]

EXPERIMENTAL RESULTS

By repeating the thermal reaction rate experiments at various temperatures, we obtained the Arrhenius plot (Fig. 3) for the overall thermal decay process of the E181Q and S186A mutants. For the E181Q mutant, over the temperature range 45-55 °C we fit the Arrhenius plot to a linear function with R = 0.9708 to yield the y-intercept of 144.4 ± 8.6 and slope of $-(4.90 \pm 0.28) \times 10^4$ K^{-1}, from which we obtained the activation energy (E_a) and the prefactor (A_{pref}) to be 97 ± 15 kcal/mol and $10^{62\pm4}$ s^{-1}, respectively. Similarly, the activation energy for thermal decay of S186A over the temperature range 45-55 °C was found to be 96 ± 8 kcal/mol and the prefactor $10^{63\pm5}$ s^{-1} (Fig. 3). Both of the mutants display lower activation energies and prefactors for thermal decay than does WT rhodopsin ($E_a \sim 114 \pm 8$ kcal/mol and $A_{pref} \sim 10^{72\pm5}$ s^{-1}).[8] For WT, similar activation energies can be extracted from previous data from Hubbard[2] and Janz and Farrens.[24] For deuterated WT rhodopsin, the thermal decay rates were found to be about a factor of 2-3 lower than for normal WT, with $E_a \sim 120 \pm 5$ kcal/mol and $A_{pref} \sim 10^{76\pm3}$ s^{-1} about the same as in H_2O within experimental uncertainty.

At lower temperatures, the picture changes dramatically. For WT, there is a distinct "elbow" in the Arrhenius plot at 46 °C (Fig. 3). Below this temperature, very different and more normal Arrhenius parameters are extracted, $E_a \sim 22 \pm 2$ kcal/mol and $A_{pref} \sim 10^{9\pm1}$ s^{-1}. This striking non-Arrhenius behavior is exhibited by the mutants, as well, but the elbow occurs at lower temperatures, $T \sim 26$ °C. For WT in D_2O, the elbow occurs at about the same temperature as for WT in H_2O. Also plotted in Fig. 3 are the rates of thermal decay of WT, E181Q and S186A in the temperature range 37-55 °C that were measured previously by Janz and Farrens.[24] Between 45 and 55 °C, our data agree quite well with those of with Janz and Farrens. For temperatures lower than 45 °C, their data also show a large change in slope. However, there are discrepancies in the absolute rates, possibly due to differences in sample preparation and reaction conditions, e.g., different buffer, different pH, etc.

The degree of melting as a function of temperature, as monitored by the ellipticity at 222 nm using circular dichroism spectroscopy, is shown in Fig. 4 for WT-H_2O, S186A, E181Q, and WT-D_2O and the results are summarized in Table I. The melting temperature of WT rhodopsin in H_2O reported here is 68.8 ± 0.5 °C, 2 °C lower than our previously reported value,[8] which is due to correction of a systematic error in calibration of the temperature control units in two different circular dichroism spectrometers used for the experiments. Figure 4 shows both mutants have T_m about 10 °C lower than that of WT rhodopsin. For WT-D_2O, we find a melting temperature of

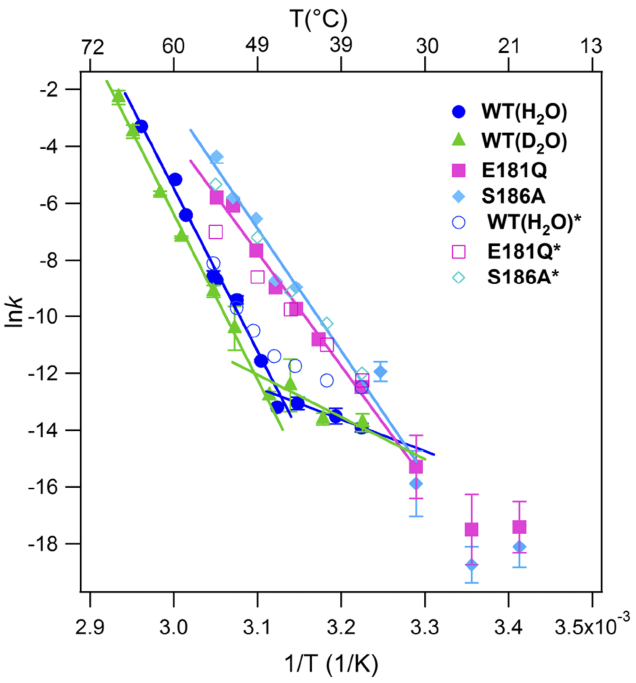

FIG. 3. Arrhenius plots obtained from the measured reaction rate constants of E181Q (pink squares), S186A (cyan diamonds), WT in H_2O (blue dots, from prior work 8), and WT in D_2O (green triangles). *Data adapted with permission from Janz and Farrens, Ref. 24.

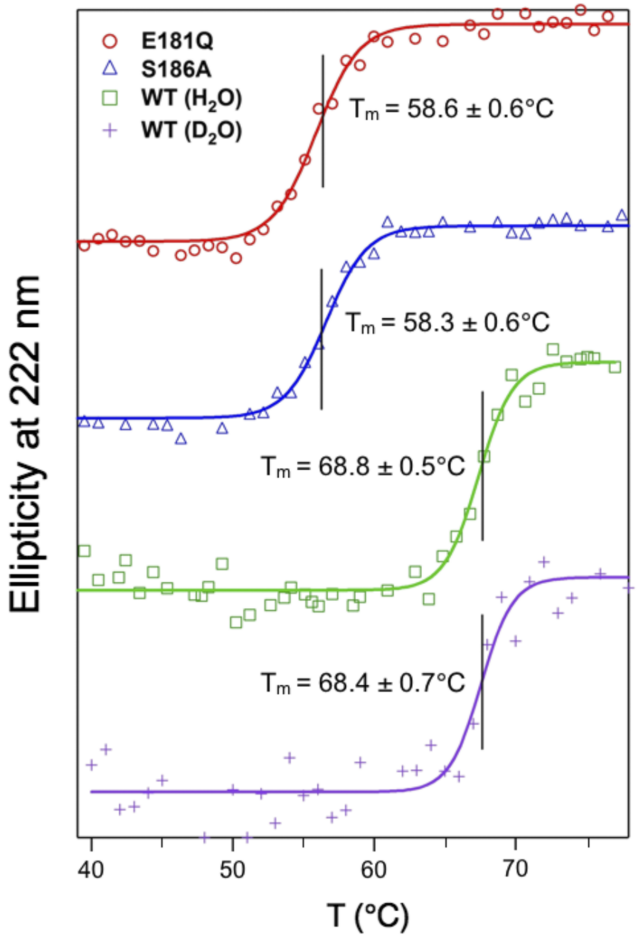

FIG. 4. Measurements of melting temperatures. The ellipticity at 222 nm (θ_{222} nm) was monitored by circular dichroism spectroscopy as temperature was scanned from 40 to 80 °C at a rate of 90 °C/h for WT rhodopsin (green, from prior work 8), S186A (blue), E181Q (red), and deuterated WT (purple) in 50 mM sodium phosphate buffer, pH 6.5, and 0.1% DDM.

TABLE I. Melting parameters.

	T_m (°C)	H_m (kcal/mol)	S_m (eu)
WT	68.8 ± 0.5	170 ± 20	496 ± 100
S186A	58.3 ± 0.4	132 ± 12	398 ± 35
E181Q	58.6 ± 0.6	128 ± 9	385 ± 29

about 68 °C, essentially the same as that for WT, but our data for WT-D_2O exhibit significant scatter, so this value is uncertain. The resulting enthalpies, ΔH_m, and entropies, ΔS_m, of melting obtained using the van't Hoff equation are summarized in Table I.

ANALYSIS

For both S186A and E181Q mutants, the measured Arrhenius activation energies for thermal decay are about 95 kcal/mol and the prefactors about 10^{62} s^{-1} over the temperature range 45–55 °C. As with WT, the activation energies are much larger than the 60 kcal/mol energy of a ~500-nm photon, and the prefactors are more than 40 orders of magnitude larger than can be attributed to the timescale of atomic motion. Nevertheless, these parameters are significantly lower than the 114 kcal/mol activation energy and 10^{72} s^{-1} prefactor we determined previously for WT.[8] This provides further evidence that the underlying mechanism responsible for the very unusual kinetics of thermal decay of rhodopsin in the higher temperature range involves the breaking of hydrogen bonds; the E181Q and S186A mutants both exhibit broken hydrogen bonds in the vicinity of the chromophore (Fig. 1), so further breakup of the HBN should involve both lower enthalpy and lower entropy. The observation that deuterated WT, which is expected to have stronger hydrogen bonds than un-deuterated WT,[13] has a somewhat lower rate of thermal decay than un-deuterated WT gives further support to the proposed mechanism.

Transition State Theory (TST)[25,26] provides a useful framework for analyzing the unusual reaction rate behavior we have observed. The TST expression for a unimolecular chemical reaction rate is

$$k_R = \left(\frac{k_B T}{h}\right) \exp\left(-\frac{\Delta G^{\ddagger}_{act}}{k_B T}\right) = \left[\left(\frac{k_B T}{h}\right) \exp\left(\frac{\Delta S^{\ddagger}_{act}}{k_B}\right)\right] \exp\left(-\frac{\Delta H^{\ddagger}_{act}}{k_B T}\right), \quad (1)$$

where k_R is the first-order rate constant (s^{-1}), k_B is Boltzmann's constant, and h is Planck's constant. $\Delta G^{\ddagger}_{act}$ is the free energy of activation, i.e., the difference between the free energy of the transition state and that of the initial reactant state, where for a system of N degrees of freedom, the transition state is an $N-1$ dimensional surface that divides reactant and product regions in configuration space. Similarly, $\Delta H^{\ddagger}_{act}$ and $\Delta S^{\ddagger}_{act}$ are the enthalpy and entropy of activation. Note that the term in square brackets directly relates the Arrhenius prefactor to the entropy of activation. Assuming for now that TST is valid for thermal decay of rhodopsin, we can use Eq. (1) to extract $\Delta H^{\ddagger}_{act}$ and $\Delta S^{\ddagger}_{act}$ from the measured rate data, as listed in Table II. Both $\Delta H^{\ddagger}_{act}$ and $\Delta S^{\ddagger}_{act}$ are significantly lower for the mutants than for WT: in the temperature range 45–55 °C for S186A, $\Delta H^{\ddagger}_{act} = 95 \pm 8$ kcal/mol and $\Delta S^{\ddagger}_{act} = 229 \pm 19$ eu; for E181Q, $\Delta H^{\ddagger}_{act} = 96 \pm 15$ kcal/mol and $\Delta S^{\ddagger}_{act} = 198 \pm 34$ eu. For WT at temperatures 52–65 °C, $\Delta H^{\ddagger}_{act} = 113 \pm 8$ kcal/mol and $\Delta S^{\ddagger}_{act} = 274 \pm 33$ eu. This again suggests that the number of hydrogen bonds broken at the transition state is somewhat less for the mutants than for WT, in agreement with expectations. As listed in Table II, for deuterated WT between 52 and 68 °C, $\Delta H^{\ddagger}_{act} = 119 \pm 5$ kcal/mol and $\Delta S^{\ddagger}_{act} = 289 \pm 45$ eu, about the same as for WT within experimental error. Note that in all four systems the entropies of activation are enormous, suggesting that the average number of broken hydrogen bonds or other intramolecular contacts must be quite high. For comparison, recent determination of the entropies of activation for isomerization of a series of polyproline peptides range from 8.8 to −9.2 eu,[27] so entropies of activation exceeding 200 eu must involve a concerted breaking of multiple bonds in the macromolecular structure of rhodopsin.

The underlying picture that emerges is an entropy-driven enhancement of the reaction rate due to disruption of the HBN in the higher temperature regimes, $T > 50$ °C for WT and $T > 40$ °C for mutants E181Q and S186A. Below these temperatures, the HBN remains essentially intact throughout the course of reaction; the energy that might be gained by disorder-induced lowering of the reaction barrier is insufficient to overcome the large free energy of breakup of the HBN. In the upper temperature range with temperatures within 20 °C below the melting temperature, the free energy of HBN breakup becomes much more modest, with the gain of entropy nearly balancing the large enthalpy of breaking hydrogen bonds. At these elevated temperatures, the HBN remains intact in the initial configuration of the reaction—the protein is still slightly below its melting temperature. However, the additional energy gained by lowering the reaction barrier is sufficient to tip the balance at the transition state, resulting in significant HBN breakup. This requires a large cost in enthalpy

TABLE II. Reaction rate parameters. The temperature used for computing $\Delta G^{\ddagger}_{act}$ was taken to be the midpoint of the indicated temperature range.

	E_{act} (kcal/mol)	A_{pref} (s^{-1})	$\Delta H^{\ddagger}_{act}$ (kcal/mol)	$\Delta S^{\ddagger}_{act}$ (e.u.)	$\Delta G^{\ddagger}_{act} = \Delta H^{\ddagger}_{act} - T\Delta S^{\ddagger}_{act}$ (kcal/mol)
WT (52-65 °C)	114 ± 8	$10^{72\pm5}$	113 ± 8	274 ± 33	23.0 @ 59 °C
WT (37-45 °C)	22 ± 2	$10^{9\pm1}$	21 ± 2	−15 ± 53	27.5 @ 40 °C
WT-D_2O (52-65 °C)	120 ± 5	$10^{76\pm3}$	119 ± 5	289 ± 45	24.3 @ 59 °C
WT-D_2O (37-45 °C)	30 ± 16	$10^{14\pm10}$	29 ± 16	10 ± 2	26.8 @ 42 °C
S186A (45-55 °C)	96 ± 8	$10^{63\pm5}$	95 ± 8	229 ± 19	23.2 @ 50 °C
E181Q (45-55 °C)	97 ± 15	$10^{62\pm4}$	96 ± 15	198 ± 34	23.9 @ 50 °C

but is mostly compensated for by the large increase in entropy. Examples of an enthalpy-entropy "compensation effect" on reaction rates and on protein-ligand binding have been reported previously,[28,29] although generally in terms of a linear free energy relationship. An enthalpy-entropy compensation effect producing a change in slope of an Arrhenius plot due to a phase transition has also been reported,[30] but the resulting elbow was far less dramatic than that reported here.

We propose a simple model that places this picture on a more quantitative footing and captures the basic observations. The underlying assumption of the model is that the environment that surrounds the reacting entity—the HBN and protein structure—can exist in only two configurations, ordered or disordered, and that the populations of the two configurations are in equilibrium at any temperature, T. This assumption is analogous to the widely invoked 2-state picture of protein folding/unfolding.[31] This assumption does not imply that the reaction path involves only two structures; indeed, the reactions of rhodopsin are known to involve several intermediates and several pathways. Our model is not inconsistent with that knowledge, but rather refers to the global environment that surrounds the reacting chromophore. The free energy of rhodopsin with its surrounding environment, ΔG_0, is $-k_BT$ times the log of the partition function,[32] i.e., the log of the sum of the Boltzmann weightings for each of the two configurations,

$$\Delta G_0 = -k_BT \ln[1 + \exp(-\beta\Delta H_D + \Delta S_D/k_B)], \qquad (2)$$

where $\beta = 1/k_BT$ and we have defined the zero of the free energy to be that of rhodopsin in its ordered configuration, resulting in its Boltzmann weighting of unity. ΔH_D and ΔS_D are, respectively, the enthalpy and entropy of the disordered configuration relative to those of the ordered configuration.

The transition state theory rate constant depends on the difference between the free energy of the initial (reactant) state and the free energy of the system when it is constrained to be at the $N-1$ dimensional dividing surface (the transition state) [Eq. (1)]. Explicit prescription of the multidimensional transition state dividing surface for this case is essentially impossible not only because of its high dimensionality but also because at least two reaction pathways (isomerization and Schiff base hydrolysis) with possibly multiple intermediates may be involved. This does not affect the validity of the model. It is sufficient for the current argument to recognize that an $N-1$ dimensional surface that completely separates reactants from products must always exist, at least in principle. Figure 5 is a schematic two-dimensional view of the extremely high dimensional potential energy surface. The "Reaction Coordinate" axis portrays the extent of thermal reaction from reactant to a transition state leading to product. Although various photoproducts (e.g., bathorhodopsin, lumirhodopsin, etc.) in the photoactivation of rhodopsin have been identified, the reaction pathway along this reaction coordinate for thermal reactions remains largely unknown. However, the model remains applicable even if there are multiple barriers and intermediates along the "Reaction Coordinate" axis, so for simplicity only a single transition state is shown in Fig. 5. The "Degree of disorder" axis is a one-dimensional simplification of the huge numbers of coordinates of the HBN. Motion from bottom to top of the figure along this axis refers to increasing disorder of the HBN, from intact at the bottom and completely disordered at the top. This is the coordinate that is simplified in the model to two states, ordered and disordered. The two-state assumption does not bear on the complexity of the reaction along the "Reaction Coordinate" axis.

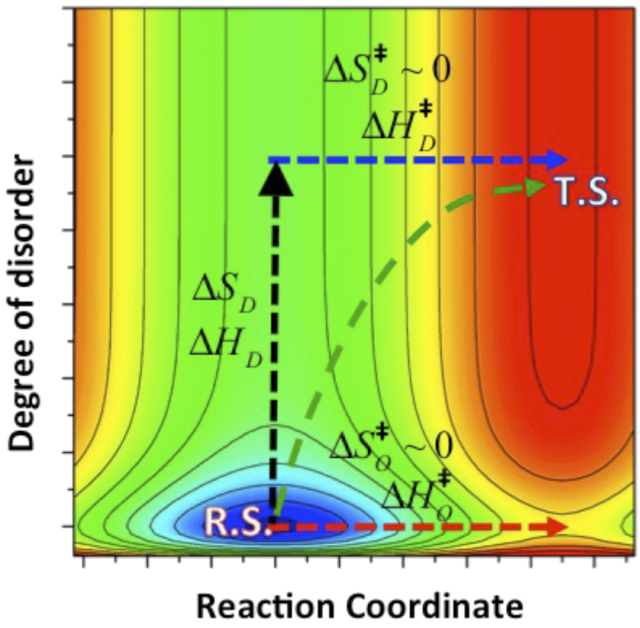

FIG. 5. 2-state model parameters. The parameters of the 2-state model are illustrated schematically. $\Delta H_O^{\ddagger}$ and $\Delta S_O^{\ddagger}$ are the enthalpy and entropy of activation when rhodopsin is in its ordered state. $\Delta H_D^{\ddagger}$ and $\Delta S_D^{\ddagger}$ are the enthalpy and entropy of activation when rhodopsin is disordered. ΔH_D and ΔS_D are the enthalpy and entropy of transition between the ordered and disordered states. Because the entropies of activation are expected to be negligible compared to the entropy of the disordering process, $\Delta S_O^{\ddagger}$, $\Delta S_D^{\ddagger} \ll \Delta S_D$, we set $\Delta S_O^{\ddagger}$ and $\Delta S_D^{\ddagger}$ to zero in applying the model, reducing the number of parameters to 4.

Putting aside for now the specific atomic coordinates that define the dividing surface, we note that the free energy of the transition state is again given by $-k_BT$ times the log of the sum of the Boltzmann probabilities for each of the two protein configurations, ordered and disordered,

$$\Delta G^{\ddagger} = -k_BT \ln\left[e^{-\beta\Delta H_O^{\ddagger} + \frac{\Delta S_O^{\ddagger}}{k_B}} + e^{-\beta\left(\Delta H_D^{\ddagger} + \Delta H_D\right) + \frac{\Delta S_D^{\ddagger} + \Delta S_D}{k_B}}\right]. \qquad (3)$$

$\Delta H_O^{\ddagger}$ and $\Delta H_D^{\ddagger}$ are the enthalpies of the ordered and disordered configurations, respectively, when constrained to the transition state dividing surface, relative to those of the unconstrained ordered and disordered configurations (Fig. 5). Similarly, $\Delta S_O^{\ddagger}$ and $\Delta S_D^{\ddagger}$ are the entropies of the ordered and disordered configurations, respectively, when constrained to the transition state dividing surface, relative to those of the unconstrained ordered and disordered configurations. We now assume for simplicity that the change of entropy between the initial state and transition state is small when the configuration of the protein is the same for both states, i.e., when both states are ordered or both are disordered ($\Delta S_O^{\ddagger} \sim 0$ and $\Delta S_D^{\ddagger} \sim 0$, Fig. 5). Accordingly, the dominant entropy change is then driven by transitions between ordered and disordered configurations, i.e., ΔS_D in Fig. 5. This entropy change can be very large, of course, and underlies the huge observed Arrhenius parameters. Setting $\Delta S_O^{\ddagger} = 0$ and

$\Delta S_D^{\ddagger} = 0$, Eq. (3) then simplifies to

$$\Delta G^{\ddagger} = -k_B T \ \ln\left[e^{-\beta \Delta H_O^{\ddagger}} + e^{-\beta\left(\Delta H_D^{\ddagger} + \Delta H_D\right) + \frac{\Delta S_D}{k_B}}\right]. \quad (4)$$

The model requires that $\Delta H_D^{\ddagger} < \Delta H_O^{\ddagger}$; i.e., the barrier to reaction is lower when rhodopsin is disordered than when it is in the ordered configuration. This provides a driving force to disorder at the transition state. At a given temperature, this results in a somewhat higher probability that the protein is disordered when it is constrained to the transition state compared to when it is in its unconstrained initial state, a critical ingredient of the model, as can be seen by comparing Eqs. (2) and (3). We have carried out QM/MM calculations to identify the transition states for WT and mutants, and to compare the computed reaction barriers when the HBN is intact versus when hydrogen bonds are broken. The calculations are based on the two-layer ONIOM (our own n-layered integrated molecular orbital and molecular mechanics) scheme,[33–36] which has been previously used for studying related retinal proteins.[8,37–43] These calculations provide interesting insights into the reaction pathways, as will be discussed in a future publication. The QM/MM results presented here focus on the isomerization pathway for which the method of identifying the transition state has already been established.[8] More detailed analyses using QM/MM calculations for both isomerization and hydrolysis pathways are in progress. Table III summarizes the QM/MM results that are directly relevant to the 2-state model presented here.

The QM/MM calculations take into account three models of the transition state:[8] one where the HBN of the minimum energy configuration remains intact, one where hydrogen bonds in the active site are disrupted, and a third where the hydrogen bonds of all water molecules in the system are disrupted. To simulate the disruption of the HBN near the active site, the MM charges of the water molecules and their hydrogen bonding partners (shown as sticks in Fig. 1) were zeroed, and the geometry was re-optimized. The atomic charges were subsequently restored, and the energy of the transition state was recomputed to obtain the barrier height. As explained in previous studies,[8] the reaction barrier determined from the QM/MM models can be partitioned into the retinal isomerization barrier (the QM barrier) and the energy required to break hydrogen bonds. As can be seen from Table III, the energy of the transition state barrier relative to that of the initial state is lowered significantly in all cases when some or all hydrogen bonds are broken, supporting the conclusion that $\Delta H_D^{\ddagger} < \Delta H_O^{\ddagger}$. Comparison of transition state structures indicates that disrupting the hydrogen bond between the protonated Schiff base and E113 carboxylate leads to an enhanced inductive electron withdrawing effect that could increase the resonance stabilization of the charge transfer transition state.[44–47] This effect may contribute, in part, to the lower reaction barrier of the transition state when the HBN becomes disrupted at higher temperatures. However, a more detailed analysis of contributions to the lower reaction barrier will be discussed in a subsequent publication.

TABLE III. QM barriers (in kcal/mol) for the isomerization process.

	WT	S186A	E181Q
HBN intact	41	39	42
HBN partially broken	27	27	26
HBN broken	28	28	27

The rate constant is given by Eq. (1), using the free energy of activation, $\Delta G_{act}^{\ddagger}$, obtained by subtracting Eq. (4) from Eq. (2). The resulting Arrhenius activation energy is

$$\begin{aligned} E_a &= -\frac{\partial \ln(k_R)}{\partial \beta} \\ &= \frac{1}{\beta} + \frac{\left(\Delta H_D^{\ddagger} + \Delta H_D - \Delta H_O^{\ddagger}\right) e^{-\beta\left(\Delta H_D^{\ddagger} + \Delta H_D - \Delta H_O^{\ddagger}\right) + \frac{\Delta S_D}{k_B}}}{1 + e^{-\beta\left(\Delta H_D^{\ddagger} + \Delta H_D - \Delta H_O^{\ddagger}\right) + \frac{\Delta S_D}{k_B}}} \\ &\quad - \frac{\Delta H_D \, e^{-\beta \Delta H_D + \frac{\Delta S_D}{k_B}}}{1 + e^{-\beta \Delta H_D + \frac{\Delta S_D}{k_B}}}. \end{aligned} \quad (5)$$

The Arrhenius prefactor is given by

$$A_{pref} = \left(\frac{k_B T}{h}\right) \exp\left[\beta(E_a - \Delta G_{act}^{\ddagger})\right]. \quad (6)$$

The model invokes 4 parameters. ΔH_D and ΔS_D of disorder and the enthalpies of the ordered configuration, $\Delta H_O^{\ddagger}$, and disordered configuration, $\Delta H_D^{\ddagger}$, when constrained to the transition state, relative to those of the corresponding initial states, i.e., the reaction barriers when ordered and disordered (see Fig. 5).

Figure 6(a) shows the natural log of our measured rate constants (s^{-1}) as a function of inverse temperature for WT, WT-D_2O, and both mutants. The solid curves are the best fits to the model [Eqs. (5) and (6)]. For WT, the values of all 4 parameters were optimized (Table IV). For the other 3 cases, the reaction barrier when the protein is disordered, $\Delta H_D^{\ddagger}$, was set to the same value as for WT because $\Delta H_D^{\ddagger}$, the reaction barrier when rhodopsin is disordered, should be essentially independent of whether or not the ordered state contains changes in the HBN.

Figure 6(a) demonstrates that the model does successfully encompass the major experimental trends. The change in the reaction pathway from an ordered to disordered transition state is reproduced, as indicated by the elbow at low temperature. At temperatures above the elbow, the calculated Arrhenius curves bend sharply upward, resulting in very high activation energies and prefactors. The values of the optimized parameters are given in Table IV. By comparison of the reaction barriers for ordered and disordered configurations, $\Delta H_O^{\ddagger}$ and $\Delta H_D^{\ddagger}$, we conclude that the rigid HBN network stabilizes the protein against reaction by about 5-7 kcal/mol. The enthalpies of disorder are similar for WT and WT-D_2O, as are the entropies of disorder, $\Delta H_D \approx 112$ kcal/mol and $\Delta S_D \approx 330$ eu. In contrast, these quantities are much smaller for the mutants, $\Delta H_D \approx 66$ kcal/mol and $\Delta S_D \approx 200$ eu. The difference of about 46 kcal/mol in the enthalpy of disorder between WT and mutants is much larger than the energy required to break the 2 or 3 hydrogen bonds that are disrupted in the mutants. This is further evidence that the HBN breakup is a concerted process involving many bonds, and suggests that this concerted action can be facilitated by initially breaking only a few bonds. The

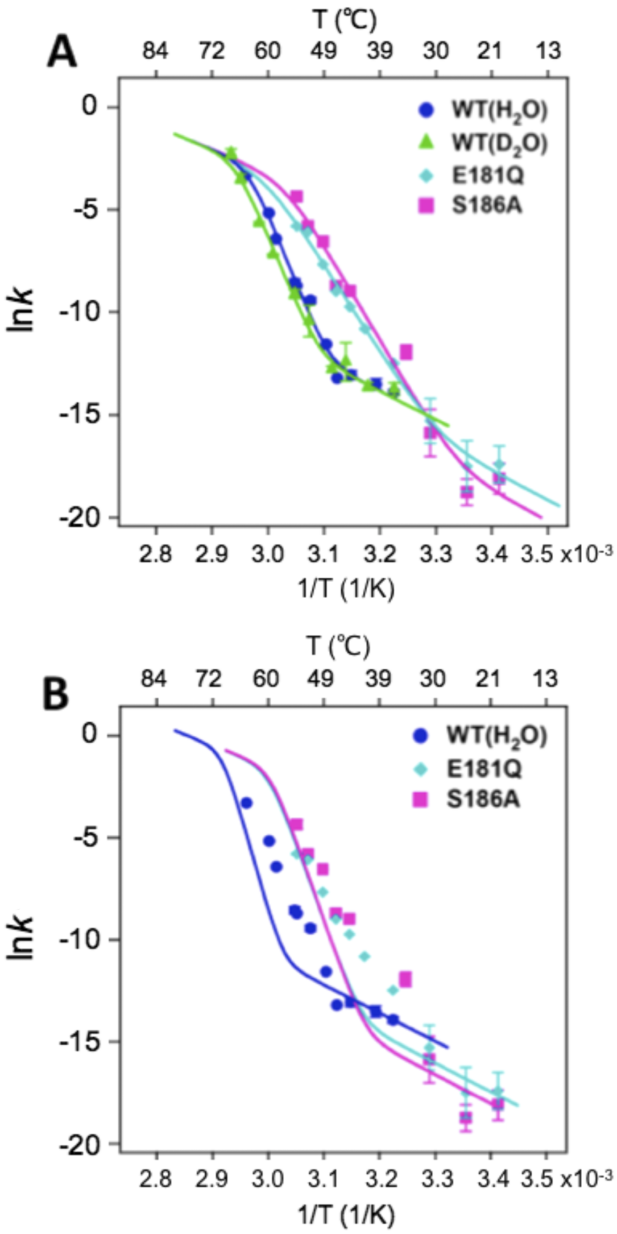

FIG. 6. (a) Fitting of Arrhenius plots of E181Q (pink squares), S186A (cyan diamonds), WT in H_2O (blue circles), and WT in D_2O (green triangles) to the model using experimentally measured data as shown in Table IV. (b) Calculated curves of Arrhenius plots of E181Q (pink squares), S186A (cyan diamonds), and WT in D_2O (green triangles) by holding $\Delta H_D^{\ddagger}$ as 21.7 kcal/mol (Table IV) and setting ΔH_D and ΔS_D equal to the melting parameters (Table I).

optimized values of the enthalpies and entropies of disorder (Table IV) are in all cases significantly lower than the corresponding enthalpies and entropies of melting determined by circular dichroism spectroscopy (Table I).

TABLE IV. Best fit parameters of the 2-state model.

	ΔH_D (kcal/mol)	ΔS_D (eu)	$\Delta H_D^{\ddagger}$ (kcal/mol)	$\Delta H_O^{\ddagger}$ (kcal/mol)
WT (H_2O)	114 ± 18	338 ± 57	21.7 ± 0.8	26.9 ± 0.2
WT (D_2O)	110 ± 11	323 ± 34	21.7	26.8 ± 0.1
E181Q	63.0 ± 5.0	189 ± 16	21.7	27.6 ± 0.2
S186A	69.9 ± 10.6	212 ± 33	21.7	28.2 ± 0.6

Figure 6(b) is the same as Fig. 6(a) but with the parameters not optimized. Rather, the parameters were chosen as follows in Fig. 6(b). The enthalpies and entropies of disorder were taken to be equal to the enthalpies and entropies of melting from Table I; $\Delta H_D = \Delta H_M$ and $\Delta S_D = \Delta S_M$. This corresponds to the unnecessary assumption that disorder is complete, i.e., the disordered state is completely melted. Therefore, these values of ΔH_D and ΔS_D can be considered upper limits, consistent with the lower values for these parameters obtained from fitting, Fig. 6(a) and Table IV. For Fig. 6(b), the reaction barrier for the disordered melted state for both WT and mutants was taken from an extrapolation of a prior measurement of the thermal rate of isomerization of 11-*cis* retinyl protonated Schiff base in solution, $\Delta H_D^{\ddagger} = 20.6$ kcal/mol.[48] For WT the final parameter, the reaction barrier at low temperature, was taken from our low temperature measurements, $\Delta H_O^{\ddagger} = 27.5$ kcal/mol. Similarly, for the mutants we obtain an estimate of $\Delta H_O^{\ddagger} = 40$ kcal/mol from our low temperature data. A WT-D_2O curve is not included in Fig. 6(b) due to the uncertainty in our experimental melting parameters for WT-D_2O.

The curves shown in Fig. 6(b), although certainly not in quantitative agreement with the experimental points, do support the underlying mechanism that at higher temperatures the reaction is promoted by an entropy-driven disordering of the protein. Distinct elbows in the Arrhenius curves are exhibited and, in the higher temperature regime, the shift between WT and mutant curves is reproduced almost quantitatively. This shift arises because the mutants have a lower temperature onset of disorder (melting) than WT, i.e., the higher temperature behavior is driven by HBN breakup.

The temperature dependent rate constants computed from the model with parameters ΔH_D and ΔS_D taken to be the enthalpies and entropies of melting, as shown in Fig. 6(b), do not fit the experimental rates accurately. This is to be expected; employing the melting parameters corresponds to the assumption that in the high temperature regime the transition state is completely melted, an extreme limit. With this choice of parameters, it is to be expected that the calculated activation energy and prefactor will be greater than the measured values, as we find. For WT, using the melting parameters in the model produces an activation energy of 190 kcal/mol and a prefactor of 10^{102} s^{-1}, compared to the experimental values of 114 kcal/mol and 10^{72} s^{-1}. These discrepancies result from the oversimplified nature of the model—the assumption that the HBN is either completely intact or completely destroyed—and may well signal that only partial melting or incomplete breakup of the HBN is required to sufficiently enhance the thermal reaction rate. It may also be that onset of disorder in the vicinity of the retinal chromophore may not be the same as the more global loss of helical content, as measured by circular dichroism spectroscopy in our melting experiments. Furthermore, the assumption of the model that rhodopsin can exist in only two states, completely ordered and completely disordered, is surely an over-simplification, neglecting the reality of partial disorder that may increase continuously with increasing temperature. Finally, the underlying equilibration assumption of transition state theory may not be completely fulfilled, possibly requiring inclusion of Kramers[25,49] or "recrossing"[25,26] corrections. TST gives an upper limit to the true equilibrium

reaction rate. For cases such as the current one that exhibit high reaction barriers, $\Delta G^{\ddagger}_{act} \gg k_B T$, the dominant temperature dependence invariably arises from the $\exp(-\Delta G^{\ddagger}_{act}/k_B T)$ term in the rate expression. Introducing Kramers diffusion terms or more sophisticated multidimensional recrossing corrections may modify the rate significantly, perhaps by a few orders of magnitude, but are very unlikely to alter the underlying picture exhibiting Arrhenius prefactors of order 10^{60}–10^{72} s^{-1}.

DISCUSSION

Through measurements of the rates of thermal decay of the rhodopsin mutants S186A and E181Q, with the aid of atomistic QM/MM calculations and a 2-state rate model, we have confirmed and quantified the contribution of the rigid HBN to the thermal stability of rhodopsin. Our observation that the activation energies and prefactors for thermal decay of the mutants are lower than those for WT, scaling approximately with the lower enthalpies and entropies of melting, strongly implicates the breaking of hydrogen bonds in the reaction pathway in the higher temperature regime. The picture that emerges is as follows: At low temperatures (below 45 °C for WT), the HBN is intact both for the reactant and the transition state. The reaction pathway does not stray far from the minimum energy path, resulting in "normal" activation energy and prefactor. For temperatures above the melting temperature (68.8 °C for WT) for which both the reactant state and transition state are disordered, there should again be a relatively small change in entropy upon reaching the transition state. While the thermal reaction rates above the melting temperature cannot be measured by our methods, we predict they would exhibit normal Arrhenius parameters because the reaction can be hypothetically considered as thermal isomerization of 11-*cis* retinal protonated Schiff base covalently attached to denatured opsin protein, but with a somewhat lower barrier than at low temperatures when the HBN impedes the reaction. In the intermediate regime (45–65 °C for WT, 40-55 °C for mutants), the transition state exhibits far more disorder than the initial state, driven by the disorder-induced lowering of the reaction barrier. This produces the very large activation energies and prefactors measured in this temperature range and is consistent with the reduction of these parameters for the mutants for which some hydrogen bonds are missing. This represents a very compelling example of the role of entropy on chemical reaction rates.

The two reactions that contribute to the overall thermal decay of rhodopsin, 11-*cis*-to-*trans* isomerization and Schiff base hydrolysis of the retinyl chromophore,[16–18] are quite localized processes in which only a relatively few atoms play a major role. The prefactors of order 10^{60}–10^{72} s^{-1} that we have observed are enormous, totally unprecedented for a localized chemical change. There are not enough degrees of freedom in a localized chemical reaction to produce the huge entropy change between the initial state and transition state. However, our results show that, in the higher range of temperatures, the thermal decay of rhodopsin is no longer a localized process; the local transformation of the chromophore drives a global disordering of the surrounding protein necessarily involving large numbers of atoms. Large prefactors for concerted motions of large systems are not unprecedented. A number of direct or indirect observations of very large Arrhenius prefactors for rates of protein unfolding/denaturation have been reported,[50] even some exceeding 10^{72} s^{-1}.[51] Interesting issues that remain to be understood for rhodopsin are how a localized motion of the chromophore can trigger widespread disorder, and the extent and nature of this disorder. The difficulty is that the process is driven by an extraordinarily high entropy of activation and, therefore, an extraordinarily large number of atomic arrangements and pathways must be involved. This precludes the possibility of uncovering any particular broken hydrogen bonds, chromophore rearrangements, etc., that may initiate the process. It is risky to even speculate how a localized transformation such as *cis-trans* isomerization can induce a global breakup of the hydrogen bonding network. As extraordinary as this may appear, the experimental and theoretical results presented here are convincing.

We conclude that the rigid HBN contributes significantly to the thermal stability of rhodopsin, 5-7 kcal/mol, and thereby to reducing dark noise and enhancing sensitivity of light detection for dim-light vision. The HBN may also play a role in eye diseases. For example, some of the point mutations in the rhodopsin gene that are associated with retinitis pigmentosa, an early symptom of which can be night blindness, are expected to break hydrogen bonds and have been shown to increase the thermal rate of isomerization.[20–22,52–54]

ACKNOWLEDGMENTS

E.C.Y.Y. acknowledges support by the National Science Foundation Career Grant No. (MCB-0955407). J.C.T. acknowledges support by DOE-BES (DE-FG02-05ER15677). V.S.B. acknowledges financial support by the National Science Foundation (Grant No. CHE 1465108) and supercomputer time from NERSC and from the High Performance Computing facilities at Yale University. Y.-N.C. is recipient of the Taiwanese Government Scholarship to Study Abroad. The authors thank Dr. Jian Liu's contribution to the early experimental work.

[1] D. A. Baylor, B. J. Nunn, and J. L. Schnapf, J. Physiol. **357**, 575–607 (1984).
[2] R. Hubbard, J. Gen. Physiol. **42**(2), 259–280 (1958).
[3] A. Reyes-Alcaraz, M. Martinez-Archundia, E. Ramon, and P. Garriga, Biophys. J. **101**(11), 2798–2806 (2011).
[4] O. Tastan, E. Yu, M. Ganapathiraju, A. Aref, A. J. Rader, and J. Klein-Seetharaman, Photochem. Photobiol. **83**(2), 351–362 (2007).
[5] J. M. Janz, J. F. Fay, and D. L. Farrens, J. Biol. Chem. **278**(19), 16982–16991 (2003).
[6] M. Yanagawa, K. Kojima, T. Yamashita, Y. Imamoto, T. Matsuyama, K. Nakanishi, Y. Yamano, A. Wada, Y. Sako, and Y. Shichida, Sci. Rep. **5**, 11081 (2015).
[7] A. V. Botelho, T. Huber, T. P. Sakmar, and M. F. Brown, Biophys. J. **91**(12), 4464–4477 (2006).
[8] Y. Guo, S. Sekharan, J. Liu, V. S. Batista, J. C. Tully, and E. C. Yan, Proc. Natl. Acad. Sci. U. S. A. **111**(29), 10438–10443 (2014).
[9] J. Li, P. C. Edwards, M. Burghammer, C. Villa, and G. F. X. Schertler, J. Mol. Biol. **343**(5), 1409–1438 (2004).
[10] T. Okada, M. Sugihara, A. N. Bondar, M. Elstner, P. Entel, and V. Buss, J. Mol. Biol. **342**(2), 571–583 (2004).
[11] T. Okada, Y. Fujiyoshi, M. Silow, J. Navarro, E. M. Landau, and Y. Shichida, Proc. Natl. Acad. Sci. U. S. A. **99**(9), 5982–5987 (2002).
[12] T. E. Angel, S. Gupta, B. Jastrzebska, K. Palczewski, and M. R. Chance, Proc. Natl. Acad. Sci. U. S. A. **106**(34), 14367–14372 (2009).
[13] S. Scheiner and M. Cuma, J. Am. Chem. Soc. **118**(6), 1511–1521 (1996).

[14]J. A. Gascon and V. S. Batista, Biophys. J. **87**(5), 2931–2941 (2004).
[15]R. B. Barlow, R. R. Birge, E. Kaplan, and J. R. Tallent, Nature **366**(6450), 64–66 (1993).
[16]J. Liu, M. Y. Liu, J. B. Nguyen, A. Bhagat, V. Mooney, and E. C. Y. Yan, J. Am. Chem. Soc. **131**(25), 8750–8751 (2009).
[17]J. Liu, M. Y. Liu, J. B. Nguyen, A. Bhagat, V. Mooney, and E. C. Y. Yan, J. Biol. Chem. **286**(31), 27622–27629 (2011).
[18]J. Liu, M. Y. Liu, L. Fu, G. A. Zhu, and E. C. Y. Yan, J. Biol. Chem. **286**(44), 38408–38416 (2011).
[19]T. P. Dryja, T. L. McGee, E. Reichel, L. B. Hahn, G. S. Cowley, D. W. Yandell, M. A. Sandberg, and E. L. Berson, Nature **343**(6256), 364–366 (1990).
[20]M. Y. Liu, J. Liu, D. Mehrotra, Y. Liu, Y. Guo, P. A. Baldera-Aguayo, V. L. Mooney, A. M. Nour, and E. C. Y. Yan, J. Biol. Chem. **288**(24), 17698–17712 (2013).
[21]M. P. Krebs, D. C. Holden, P. Joshi, C. L. Clark, A. H. Lee, and S. Kaushal, J. Mol. Biol. **395**(5), 1063–1078 (2010).
[22]D. Toledo, E. Ramon, M. Aguila, A. Cordomi, J. J. Perez, H. F. Mendes, M. E. Cheetham, and P. Garriga, J. Biol. Chem. **286**(46), 39993–40001 (2011).
[23]P. Atkins and J. D. Paula, *Physical Chemistry*, 8th ed. (W. H. Freeman and Company, 2006).
[24]J. M. Janz and D. L. Farrens, J. Biol. Chem. **279**(53), 55886–55894 (2004).
[25]P. Hanggi, P. Talkner, and M. Borkovec, Rev. Mod. Phys. **62**(2), 251–341 (1990).
[26]J. I. Steinfeld, J. S. Francisco, and W. L. Hase, *Chemical Kinetics and Dynamics*, 2nd ed. (Prentice Hall, Upper Saddle River, NJ, USA, 1999).
[27]Y. J. Lin, L. K. Chu, and J. C. Horng, J. Phys. Chem. B **119**(52), 15796–15806 (2015).
[28]S. L. Jacques, J. Biomed. Opt. **11**(4), 041108 (2006).
[29]L. Movileanu and E. A. Schiff, Monatsh. Chem. **144**(1), 59–65 (2013).
[30]P. J. Estrup, E. F. Greene, M. J. Cardillo, and J. C. Tully, J. Phys. Chem. **90**(17), 4099–4104 (1986).
[31]R. Zwanzig, Proc. Natl. Acad. Sci. U. S. A. **94**(1), 148–150 (1997).
[32]K. A. Dill and S. Bromberg, *Molecular Driving Forces* (Garland Science, 2003).
[33]F. Maseras and K. Morokuma, J. Comput. Chem. **16**(9), 1170–1179 (1995).
[34]S. Dapprich, I. Komáromi, K. S. Byun, K. Morokuma, and M. J. Frisch, J. Mol. Struct.: THEOCHEM **461-462**, 1–21 (1999).
[35]T. Vreven, K. S. Byun, I. Komáromi, S. Dapprich, J. A. Montgomery, K. Morokuma, and M. J. Frisch, J. Chem. Theory Comput. **2**(3), 815–826 (2006).
[36]D. Bakowies and W. Thiel, J. Phys. Chem. **100**(25), 10580–10594 (1996).
[37]S. Sekharan, A. Altun, and K. Morokuma, J. Am. Chem. Soc. **132**(45), 15856–15859 (2010).
[38]S. Sekharan, K. Katayama, H. Kandori, and K. Morokuma, J. Am. Chem. Soc. **134**(25), 10706–10712 (2012).
[39]S. Sekharan and K. Morokuma, J. Am. Chem. Soc. **133**(47), 19052–19055 (2011).
[40]S. Sekharan and K. Morokuma, J. Am. Chem. Soc. **133**(13), 4734–4737 (2011).
[41]R. Pal, S. Sekharan, and V. S. Batista, J. Am. Chem. Soc. **135**(26), 9624–9627 (2013).
[42]S. Sekharan, V. L. Mooney, I. Rivalta, M. A. Kazmi, M. Neitz, J. Neitz, T. P. Sakmar, E. C. Y. Yan, and V. S. Batista, J. Am. Chem. Soc. **135**(51), 19064–19067 (2013).
[43]S. Sekharan, J. N. Wei, and V. S. Batista, J. Am. Chem. Soc. **134**(48), 19536–19539 (2012).
[44]S. Gozem, I. Schapiro, N. Ferré, and M. Olivucci, Science **337**(6099), 1225 (2012).
[45]S. Rinaldi, F. Melaccio, S. Gozem, F. Fanelli, and M. Olivucci, Proc. Natl. Acad. Sci. U. S. A. **111**(5), 1714–1719 (2014).
[46]A. Zen, E. Coccia, S. Gozem, M. Olivucci, and L. Guidoni, J. Chem. Theory Comput. **11**(3), 992–1005 (2015).
[47]I. Schapiro and F. Neese, Comput. Theor. Chem. **1040-1041**, 84–98 (2014).
[48]D. Lukton and R. R. Rando, J. Am. Chem. Soc. **106**(1), 258–259 (1984).
[49]H. A. Kramers, Physica **7**, 284–304 (1940).
[50]M. Goyal, T. K. Chaudhuri, and K. Kuwajima, PLoS One **9**(12), e115877 (2014).
[51]L. S. Zamorano, D. G. Pina, J. B. Arellano, S. A. Bursakov, A. P. Zhadan, J. J. Calvete, L. Sanz, P. R. Nielsen, E. Villar, O. Gavel, M. G. Roig, L. Watanabe, I. Polikarpov, and V. L. Shnyrov, Biochimie **90**, 1737–1749 (2008).
[52]R. McKeone, M. Wikstrom, C. Kiel, and P. E. Rakoczy, Mol. Vision **20**, 183–199 (2014).
[53]J. M. Janz and D. L. Farrens, Vision Res. **43**(28), 2991–3002 (2003).
[54]E. P. Rakoczy, C. Kiel, R. McKeone, F. Stricher, and L. Serrano, J. Mol. Biol. **405**(2), 584–606 (2011).